Full Paper
doi.org/10.1002/chem.202000266

Phosphorus Chemistry | *Hot Paper*

A Phosphinine-Derived 1-Phospha-7-Bora-Norbornadiene: Frustrated Lewis Pair Type Activation of Triple Bonds

Julia Leitl,[a] Andrew R. Jupp,[b] Evi R. M. Habraken,[b] Verena Streitferdt,[c] Peter Coburger,[a] Daniel J. Scott,[a] Ruth M. Gschwind,*[c] Christian Müller,*[d] J. Chris Slootweg,*[b] and Robert Wolf*[a]

Abstract: Salt metathesis of 1-methyl-2,4,6-triphenylphosphacyclohexadienyl lithium and chlorobis(pentafluorophenyl)borane affords a 1-phospha-7-bora-norbornadiene derivative **2**. The C≡N triple bonds of nitriles insert into the P–B bond of **2** with concomitant C–B bond cleavage, whereas the C≡C bonds of phenylacetylenes react with **2** to form λ^4-phosphabarrelenes. Even though **2** must formally be regarded as a classical Lewis adduct, the C≡N and C≡C activation processes observed (and the mild conditions under which they occur) are reminiscent of the reactivity of frustrated Lewis pairs. Indeed, NMR and computational studies give insight into the mechanism of the reactions and reveal the labile nature of the phosphorus–boron bond in **2**, which is also suggested by detailed NMR spectroscopic studies on this compound. Nitrile insertion is thus preceded by ring opening of the bicycle of **2** through P–B bond splitting with a low energy barrier. By contrast, the reaction with alkynes involves formation of a reactive zwitterionic methylphosphininium borate intermediate, which readily undergoes alkyne 1,4-addition.

Introduction

1-*R*-Phosphacyclohexadienyl anions (**A**, Figure 1, also sometimes referred to as λ^4-phosphinine anions) present a promising, yet underutilised platform for accessing diverse functionalised organophosphorus molecules.[1] Anions **A** can easily be prepared from organolithium or Grignard reagents and aromatic λ^3,σ^2-phosphinines and show ambidentate character toward various electrophiles, including transition-metal centers. With "soft" alkylating agents, such as CH_3I, an S_N2 reaction with the phosphorus atom lone pair typically results in formation of a 1,1-disubstituted λ^5-phosphinine (type **B**). "Hard" electrophiles such as acylium ions or protons usually attack at the more electron-rich C4- or C2-positions of the heterocycle (type **C** and **D**, respectively), affording the corresponding 1,2- or 1,4-dihydrophosphacyclohexadienes.[2]

For example, protonation (type **D**) usually proceeds exclusively at the C2-position of the λ^4-phosphinine anion.[3] It has been proposed that typically 1,1-products (**B**) are thermodynamically favoured, whereas 1,2- and 1,4-products (**C** and **D**) arise through kinetically controlled reactions.[2b] λ^4-Phosphinines can also serve as anionic ligands for transition metal complexes. Depending on the nature of the ring-substitution pattern and the metal fragment, η^1-, η^2-, η^5- or even η^1:η^5-coordination (type **E**) can be observed.[4] Some of these coordination compounds have found applications in homogeneous catalysis, such as [(1,5-cod)Rh(η^5-1-*t*Bu-2,4,5,6-Ph-PC_5H)] for the Rh-catalysed hydroformylation of olefins.[4b–e]

As part of our program to study the chemistry of reactive and catalytically active phosphinine and phosphacyclohexadienyl complexes,[5] we anticipated that the reaction of λ^4-phosphinine anions **A** with chloroboranes would lead to neutral, phosphinine-based heterocycles that exhibit both a Lewis basic phosphorus atom moiety and an additional Lewis acidic boryl site.[5b] Related systems have attracted much attention lately as so-called "frustrated Lewis pairs" (FLPs), which typically consist of trivalent alkyl or aryl phosphine and borane

[a] J. Leitl, Dr. P. Coburger, Dr. D. J. Scott, Prof. Dr. R. Wolf
Institute of Inorganic Chemistry
University of Regensburg
93040 Regensburg (Germany)
E-mail: robert.wolf@ur.de

[b] Dr. A. R. Jupp, Dr. E. R. M. Habraken, Dr. J. C. Slootweg
van 't Hoff Institute for Molecular Sciences
University of Amsterdam
Science Park 904, PO Box 94157
1090 GD Amsterdam (The Netherlands)
E-mail: j.c.slootweg@uva.nl

[c] V. Streitferdt, Prof. Dr. R. M. Gschwind
Institute of Organic Chemistry
University of Regensburg
93040 Regensburg (Germany)
E-mail: ruth.gschwind@ur.de

[d] Prof. Dr. C. Müller
Institute of Chemistry and Biochemistry
Freie Universität Berlin
Fabeckstr. 34/36, 14195 Berlin (Germany)
E-mail: c.mueller@fu-berlin.de

Supporting information and the ORCID identification number(s) for the author(s) of this article can be found under: https://doi.org/10.1002/chem.202000266.

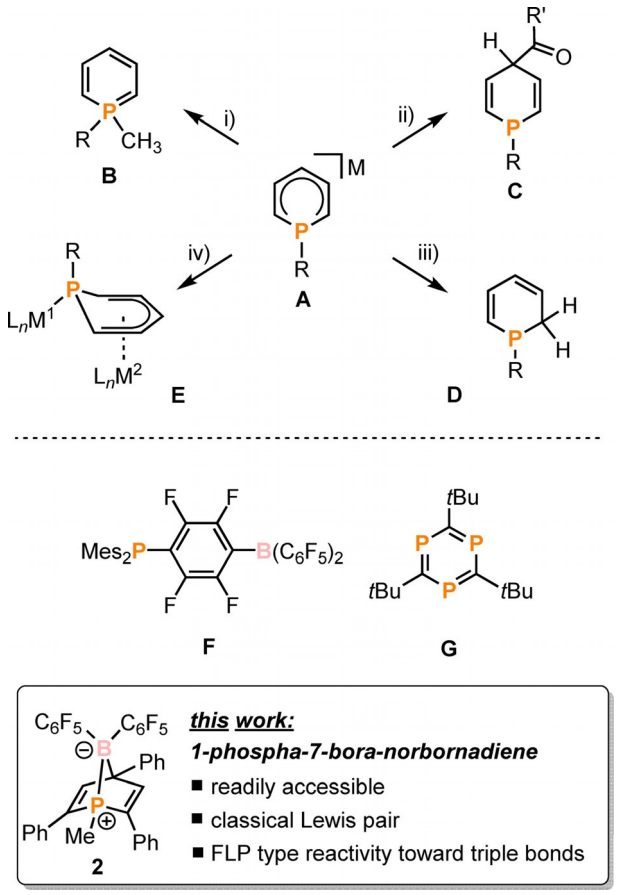

Figure 1. A generic 1-*R*-phosphacyclohexadienyl anion **A** and its reactivity toward various electrophiles; the first reported P/B FLP (**F**); a triphosphabenzene derivative that displays FLP-like reactivity (**G**). Reagents: i) CH_3I, ii) R′COCl, iii) H^+, iv) $M^1L_n = M^2L_n = Rh(1,5\text{-cod})$, cod = cycloocta-1,5-diene; R = aryl or alkyl substituents.

units.[6] For example, Stephan's groundbreaking intramolecular FLP $Mes_2PC_6F_4B(C_6F_5)_2$ (**F**, Figure 1) displays unquenched reactivity at the Lewis acidic borane and basic phosphine moieties, allowing it to split dihydrogen reversibly,[7] and similar systems also react with other small molecules such as CO_2.[8]

Despite the ubiquity of sp^3-hybridised λ^3,σ^3-phosphorus Lewis bases in FLP chemistry, the use of phosphorus bases in other coordination environments remains essentially unexplored, except for one recent example reported by Stephan and co-workers who showed that 2,4,6-tri-*tert*-butyl-1,3,5-triphosphinine (**G**, Figure 1) is able to activate dihydrogen in an FLP type manner.[9] Herein we describe the synthesis, thorough characterisation and reactivity of a bicyclic 1-phospha-7-bora-norbornadiene **2**, which possesses a direct, polar P–B bond. Despite formally being a classical Lewis adduct, compound **2** displays characteristic FLP-like behaviour due to the presence of easily thermally-accessible ring-opened isomers, which contain unquenched Lewis acidic and Lewis basic sites. As a result, **2** behaves as a masked FLP and readily activates the strong C≡N and C≡C triple bonds of nitriles and phenylacetylenes, forming unusual nitrile insertion and alkyne addition products.

Results and Discussion

Synthesis, characterisation and mechanism of formation of 1-phospha-7-bora-norbornadiene 2

Taking the known reactivity of **A** with electrophiles into account (Figure 1), it was anticipated that a chloroborane could be used to install a strongly electrophilic boron center onto a phosphacyclohexadienyl scaffold by salt elimination. On this basis, the simple salt $Li[1\text{-Me-}PC_5H_2Ph_3]$ (**1**) was chosen as a starting material, which is easily prepared from methyl lithium and 2,4,6-triphenylphosphinine (TPP, Scheme 1).[2c] Upon treatment of **1** with $(C_6F_5)_2BCl$ at $T = -35\,^{\circ}C$ in *n*-hexane, a colour change from deep pink to orange was observed, with concomitant precipitation of an orange solid. Following filtration, dissolution of the remaining solid in diethyl ether, refiltration (to remove LiCl) and removal of solvent, a new compound **2** was isolated as a bright orange solid in 35% yield. Compound **2** was characterised by single crystal X-ray diffraction, NMR and UV–Vis spectroscopy as well as elemental analysis, all of which provided data that are consistent with the molecular structure depicted in Scheme 1 (vide infra). In particular, single crystals of **2**, suitable for X-ray diffraction, were obtained by slow evaporation of the solvent from a solution of **2** in *n*-hexane at room temperature. Crystallographic characterisation revealed a hitherto unknown hetero-norbornadiene structure (Figure 2), in which the boron atom has adopted a bridging position between the P1 and C4 positions of the phosphorus heterocycle. This unusual structure (c.f. **B**–**D**) can be attributed to the

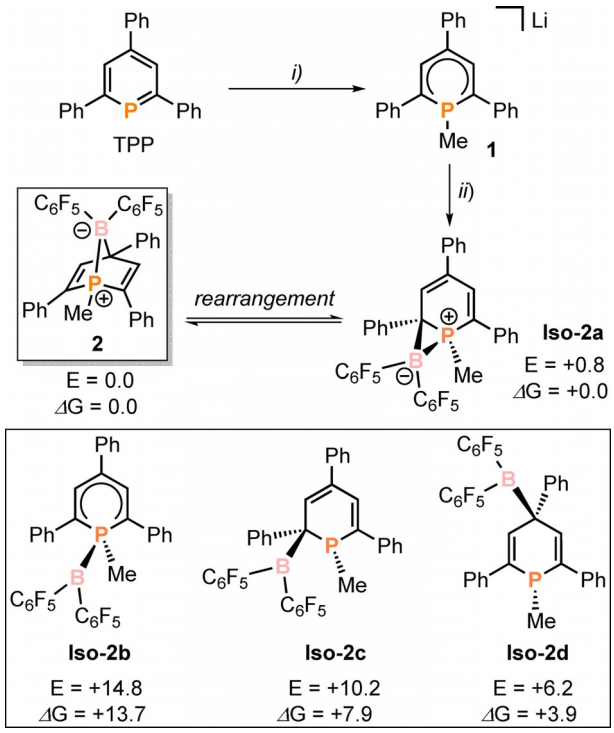

Scheme 1. Synthesis of **2** through **1** and **Iso-2a**; reagents and conditions: i) MeLi (Et_2O, −78 °C), ii) $(C_6F_5)_2BCl$/−LiCl (RT, *n*-hexane). Relative wB97X-D/6–311 + G** electronic energies (ΔE in kcal mol^{-1}) and free energies (ΔG in kcal mol^{-1}) for possible isomers of **2** (**Iso-2a**–**Iso-2d**).

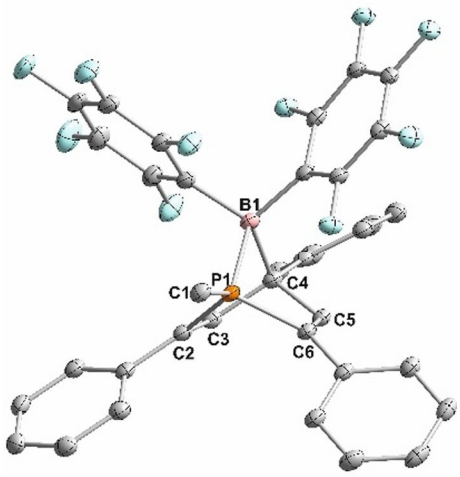

Figure 2. Molecular structure of **2** in the single crystal. Displacement ellipsoids are shown at the 40% probability level; H atoms are omitted for clarity; selected bond lengths [Å] and angles [°]: P1–B1 1.9894(19); P1–C1 1.8025(17); B1–C4 1.721(2); P1–C2 1.8146(17); P1–C6 1.8081(17); C2–C3 1.344(3); C6–C5 1.336(2); C1-P1-B1 129.51(8); C2-P1-C6 101.44(8); P1-B1-C4 84.58(10).

doubly electrophilic nature of the chloroborane, which allows the formation of a second, bridging interaction that is not available to most other main group electrophiles. It is worth noting that phospha-norbornadienes have received significant attention as ligands in homogeneous catalytic reactions, for example, the hydrogenation and hydroformylation of alkenes as well as Heck reactions.[10] Furthermore, compound **2** is a rare example of a hetero-norbornadiene based on both phosphorus and boron.[11] Derivatives with phosphorus and another additional heteroatom in the norbornadiene scaffold are scarce, although Streubel and co-workers have described a 7-aza-1-phospha-norbornadiene and group 13 7-metalla-1,4-diphospha-norbornadienes (mechanistic and reactivity studies of which have unfortunately not been reported).[12] Also of note are the very mild conditions used for the preparation of **2**, which contrasts with the much more forcing conditions required to prepare many other 1-phospha-norbornadiene derivatives.[13]

Whereas the P1–B1 distance of 1.9894(19) Å in **2** is in the range of phosphorus boron single bonds (sum of covalent radii = 1.96 Å),[14] the B1–C4 bond is slightly elongated compared both to the sum of the covalent radii (1.721(2) Å versus 1.60 Å)[14] and to previously reported 7-bora-norbornadienes (about 1.641 Å),[15] suggesting significant strain in the bicyclic structure.[16] A similar phenomenon was observed by Braunschweig and co-workers for a heptaphenyl-7-borabicycloheptadiene N-heterocyclic carbene adduct (B–C: 1.743 Å), in which the boron atom is also four-coordinate.[17] Also of note are the C2–C3 and C5–C6 distances within the phosphorus heterocycle, which are characteristic of C=C double bonds (1.344(3) and 1.336(3) Å, respectively).[18]

The $^{31}P\{^{1}H\}$ NMR spectrum of **2** shows a poorly resolved signal at $\delta(\text{ppm}) = +18.6$ at room temperature (see Figures S3 and S79), whereas the ^{11}B spectrum reveals a resonance at $\delta(\text{ppm}) = +14.1$ consistent with four-coordinate boron (see Figures S5, S82 and S84).

To elucidate the pathway for the formation of **2**, variable temperature (VT) ^{11}B and $^{31}P\{^{1}H\}$ NMR reaction monitoring was performed, alongside DFT calculations. ^{11}B NMR spectra recorded during the reaction of **1** and $(C_6F_5)_2BCl$ revealed not only the formation of product **2** ($\delta(\text{ppm}) = +13$) but also of an additional species, **Iso-2a**, characterised by a resonance at $\delta(\text{ppm}) = -25$ (Figure S82). Further information on the reaction was obtained by $^{31}P\{^{1}H\}$ NMR monitoring (see Figure 3a; see Supporting Information for experimental details and Figure S79 for further spectra) which showed that **1** ($\delta(\text{ppm}) = -72.5$) is fully converted even at low temperature. The signal of product **2** appears within minutes even at 193 K (see Figure 3a). However, another intense and broad signal can be observed at $\delta(\text{ppm}) = -102$ (**Iso-2a** in Figure 3a), which converts into **2** as the temperature is increased, suggesting an intermediate species. Calculations at the TPSS/IGLO-III CPCM(THF) level of theory showed that the experimental ^{31}P shift of −102 ppm and the ^{11}B shift of −25 ppm both fit well to a proposed three-membered B–C–P ring species, and this structure is consequently assigned to **Iso-2a** (see Table 1 and Scheme 1). Calculations also suggested that this structure should be very similar in energy to **2**, and indeed, NMR analysis of even authentic samples of crystalline **2** showed the presence of minor amounts of **Iso-2a**, consistent with reversible isomerisation in solution.

Table 1. Calculated (calcd) ^{31}P and ^{11}B NMR shifts [ppm] and coupling constants $J_{P\text{-}B}$ [Hz] at the TPSS/IGLO-III CPCM(THF) level of theory. The calculated absolute shieldings of compound **2** served as reference for the other compounds. Experimental (exp) chemical shifts of **2** and **Iso-2a** are also given.

	2	**Iso-2a**	**Iso-2b**	**Iso-2c**	**Iso-2d**
$\delta(^{31}P)$	+18 (exp)	−98 (calcd) −102 (exp)	−16	−38	−43
$\delta(^{11}B)$	+14 (exp)	−26 (calcd) −25 (exp)	+32	+66	+47
$J_{P\text{-}B}$	87	6			

Given the known reactivity of λ^4-phosphinine anions with electrophiles shown in Scheme 1, other plausible structures **Iso-2b**–**Iso-2d** were also investigated as possible intermediates. DFT calculations at the ωB97X-D/6–311+G** level showed that isomers with a tricoordinate boryl substituent in the 1-, 2- or 4-position are all higher in energy than **2** or **Iso-2a** (see Scheme 1), and therefore less likely to accumulate during the course of the reaction. This is corroborated by a chemical shift analysis of these structures (Table 1), which predicts significantly different NMR shifts for the isomers **Iso-2b**–**Iso-2d** than those observed experimentally. Nevertheless, it should be noted that structure **Iso-2d** in particular is predicted to be thermally accessible at even modest temperatures on the basis of the above calculations.

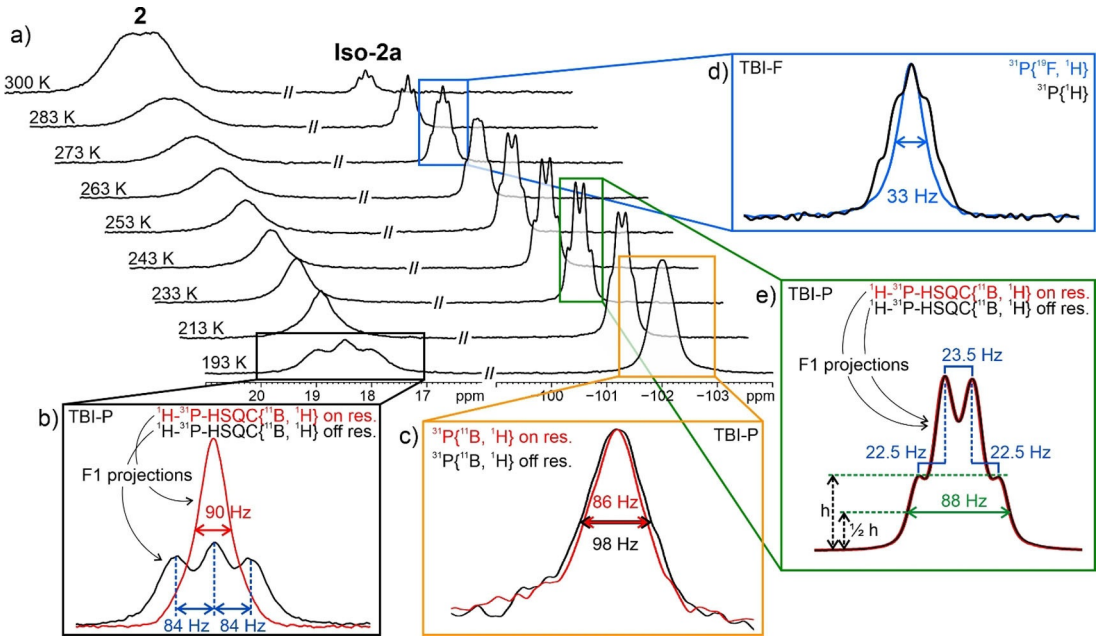

Figure 3. a) ^{31}P{^{1}H} NMR monitoring (starting from 193 K and warming up to 300 K) of the reaction of **1** with $(C_6F_5)_2BCl$ (see Supporting Information for full spectra, Figure S79). The spectral regions of **2** and **Iso-2a** are displayed with the same expansion and intensity scaling. b) Overlaid F1 (indirect dimension) projections of a ^{1}H–^{31}P HSQC with simultaneous ^{11}B and ^{1}H decoupling in F1 and ^{31}P decoupling in F2 (direct dimension) acquired in the region of **2** (better signal/noise compared to 1d ^{31}P spectrum, see S81 in Supporting Information for pulse program). ^{11}B decoupling was applied on resonance (red) and off resonance (black). The spectra were acquired on a TBI-P probe. c) Overlaid 1d ^{31}P spectra with simultaneous ^{11}B and ^{1}H decoupling. ^{11}B decoupling was applied on resonance (red) and off resonance (black). The spectra were adjusted to same height for a better comparison of line widths. The spectra were acquired on a TBI-P probe. d) Overlaid 1d ^{31}P spectra with ^{1}H decoupling only (black) and simultaneous ^{19}F and ^{1}H decoupling (blue). The spectra were adjusted to same height for a better comparison of line widths (see also S80 in Supporting Information). The spectra were acquired on a TBI-F probe. e) Overlaid F1 projections of a ^{1}H–^{31}P HSQC with simultaneous ^{11}B and ^{1}H decoupling in F1 and ^{31}P decoupling in F2 acquired in the region of **Iso-2a**. The spectra were acquired on a TBI-P probe.

Variable temperature NMR characterisation of isomers 2 and Iso-2a

During VT NMR monitoring of the formation of **2** it was noted that the ^{31}P{^{1}H} resonances for both **2** and **Iso-2a** show complex temperature-dependent behaviour. To understand these observations (and also further support the structural assignment of **Iso-2a**) an in-depth analysis of the relevant multinuclear VT NMR spectra was carried out.

In the ^{31}P{^{1}H} NMR spectra, the multiplicities of the ^{31}P{^{1}H} signals of both **2** and **Iso-2a** change upon warming from 193 K (see Figure 3a). Over the entire temperature range examined, the signal of **2** is dominated by scalar couplings to ^{11}B and the quadrupolar relaxation of ^{11}B. This was proven by simultaneously ^{11}B and ^{1}H decoupled ^{31}P spectra (see ^{31}P{^{11}B, ^{1}H} spectrum in Figure 3b), which show a clear collapse of the triplet with a coupling constant of $^{1}J_{PB}=84$ Hz at 193 K. Additional ^{31}P{^{19}F, ^{1}H} experiments did not change the signal of **2** (Figure S80), which is reasonable for scalar couplings being significantly smaller than the half line width ($\nu_{1/2}=90$ Hz). With increasing temperature, the ^{31}P{^{1}H} signal of **2** becomes first a singlet and then a very broad doublet from 300 K upwards (for a temperature row between 193 K and 333 K of **2**, see Figure S83). The corresponding ^{11}B signal changes from a very broad singlet to a sharper doublet at 300 K corroborating the large scalar coupling constant between ^{11}B and ^{31}P ($^{1}J_{PB}=$ 90 Hz, see Figure S82), which is accompanied by a downfield shift. Similar behaviour was observed in a temperature screening of a solution containing exclusively **2** in which the ^{11}B signal of **2** started out as being relatively sharp at 193 K (see Figure S84), then first broadened and subsequently narrowed during a steady temperature increase. Again, this went along with a downfield shift (around 1.4 ppm, see Figure S84). The line broadening associated with a downfield shift is probably related to a coalescence of **2** with another species downfield shifted relative to **2**. Given the relatively low energy predicted for isomer **Iso-2d** (vide supra) this is likely to be the relevant species, and these variable temperature measurements therefore further hint at the labile nature of the B–P bond in **2** (a ^{11}B shift of 1.4 ppm for **2** would correspond to the presence of around 4% of **Iso-2d**; see Supporting Information for calculation). Within this exchange the P–B bond is broken and re-established, which may alter $^{1}J_{PB}$ and could therefore give rise to the observed change in shape of the ^{31}P{^{1}H} signal of **2** during temperature increase (see Figure 3a).

The ^{31}P{^{1}H} signal of **Iso-2a** at δ(ppm) = −102 exhibits a significantly different response upon temperature increase. At 193 K quadrupolar relaxation seems to dominate producing a broad singlet ($\nu_{1/2}=98$ Hz). During warm-up, this signal becomes sharper (Figure S79) and develops a quartet splitting which at higher temperatures converts into a quintet (see Figure 3a and Figure S79). ^{31}P NMR with simultaneous ^{19}F and ^{1}H decoupling revealed that the splitting results from coupling to ^{19}F (see ^{31}P{^{19}F, ^{1}H} in Figure 3d). The fact that different multip-

lets are observed at altered temperatures may be attributed to the presence of two chemically-distinct, hindered C_6F_5 rings, each of which may independently suffer from hindered rotation about its B–C bond (of the structures proposed in Scheme 1 this is only the case for **Iso-2a**). Whereas the *ortho* (and *meta*) fluorines of a freely rotating ring would have identical scalar couplings to phosphorus, those in a hindered ring may have different couplings. Thus, similar coupling of ^{31}P to both fluorines of one freely-rotating C_6F_5 ($^4J_{PF}=22.5$ Hz) and only one fluorine of a hindered C_6F_5 ($^4J_{PF}=23.5$ Hz) would give rise to the observed quartet (see Figure 3e). At elevated temperatures, stronger rotation of the fluoroaryls and/or rapid P–B-bond opening and closing presumably results in a similar scalar coupling of ^{31}P to all four *ortho* fluorines, creating a quintet coupling pattern. $^{31}P\{^{11}B,^1H\}$ measurements at 193 K showed a small reduction in line width (see Figure 3c), whereas at 233 K no change in line width or multiplet structure was observed (see Figure 3e). This implies that at 193 K the ^{31}P signal of **Iso-2a** is dominated by the quadrupolar relaxation effects of ^{11}B. In contrast, at higher temperatures there is an apparently smaller influence of ^{11}B on the line width which is now mainly dominated by coupling to ^{19}F. Calculations at the TPSS/IGLO-III CPCM(THF) level of theory revealed a $^1J_{PB}$ of 6 Hz for **Iso-2a** (see Table 1) which fits well to the observation of a small change in line width at 193 K and no change at 233 K. Verifying the P–B bond in **Iso-2a** by ^{31}P–^{11}B HMQC was not successful due to the extremely broad ^{11}B signals associated with very short transverse relaxation times (T_2). A ^1H–^{31}P HSQC spectrum revealed the expected break in symmetry of the heterocycle in **Iso-2a** compared to **2** since the protons bound to the P-heterocycle exhibit different shifts and ^1H–^{31}P coupling constants (Figure S81). Taken collectively, these NMR observations therefore strongly support the proposed structure of **Iso-2a**.

Reactivity of 2 toward nitriles

Although the solid-state structure of **2** clearly indicated the formation of a classical Lewis acid–base adduct involving the phosphorus and the boron atom, XRD, DFT and VT NMR analyses all suggested that reversible, thermal P–B bond cleavage could plausibly provide access to a ring-opened isomer **Iso-2d** possessing unquenched acidic and basic sites. It was thus anticipated that FLP-type behaviour might still be observable for compound **2**, in line with both our initial predictions and results reported previously for some other boron-based Lewis adducts.[19] Indeed, more direct evidence that such reactivity is possible was observed during attempts to dissolve samples of **2** in deuterated acetonitrile for NMR purposes, which led to a clear colour change from orange to deep green. Although activation of other unsaturated C=X bonds by FLPs is very well established, reports of nitrile activation are remarkably scarce, with this having been achieved only for a family of geminal phosphinoboranes reported by Wagner and Slootweg, which reacted to generate five-membered cyclic structures, and a single, more elaborate enamine/borane system reported by Erker et al.[20] Nevertheless, addition of acetonitrile to a solution of **2** in diethyl ether at RT resulted in an immediate colour change to deep green and the $^{31}P\{^1H\}$ NMR spectrum of the reaction mixture indicated the selective formation of a single new species **3a** (Scheme 2), as evidenced by a sharp singlet resonance at $\delta(\text{ppm})=+0.6$, that is shifted to higher field relative to **2** (Figure S11). In the proton-coupled ^{31}P NMR spectrum this signal appears as a complex multiplet (Figure S12). Additionally, the $^{11}B\{^1H\}$ NMR spectrum shows a broad signal at $\delta(\text{ppm})=+21.9$ that is shifted to lower field relative to **2**, which is qualitatively consistent with a change from four- to three-coordinate boron. Single crystals were grown by slow evaporation of an *n*-hexane solution of **3a** at room temperature. Gratifyingly, the crystallographic characterisation confirmed activation of the nitrile triple bond, although this was unexpectedly accompanied by cleavage of not just the P–B bond but also the C–B bond of **2** (Figure 4) with the nitrile having formally inserted into the former. The resulting BCN moiety is almost linear (C7-N1-B1 172°), and the N1–B1 distance is significantly shortened (1.367(2) Å) compared to common N–B single bonds (1.57 Å),[14] suggesting some multiple bond character due to donation of electron density from the nitrogen lone pair into the empty p orbital on boron. The nitrile-derived C7–N1 distance is in the range of typical C–N double bonds (1.251(2) Å),[18] and the P1–C7 separation (1.8822(17) Å) is in the range of single bonds according to the sum of the covalent radii (P–C 1.86 Å).[14]

Other substituted nitriles were subsequently employed in similar reactions, yielding compounds **3b**–**3e** (Scheme 2) as

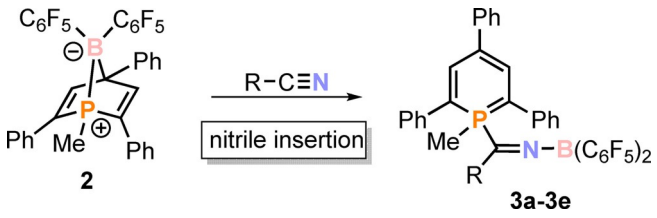

Scheme 2. Synthesis of nitrile insertion products **3a**–**3e** (yields of isolated compounds are given in parentheses in this caption): **3a**: R = Me (33%), **3b**: R = Ph (64%), **3c**: R = 3,5-$Br_2C_6H_3$ (43%), **3d**: R = CH_2Cl (39%), **3e**: R = Et (41%).

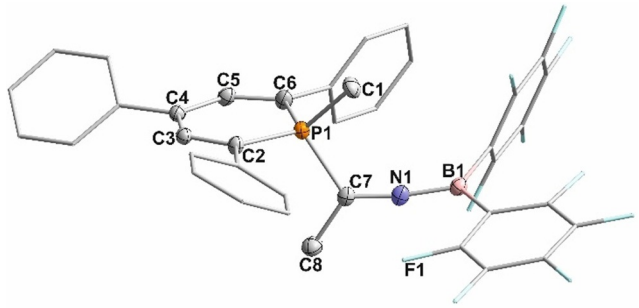

Figure 4. Molecular structure of **3a** in the single crystal. Displacement ellipsoids are shown at the 40% probability level; H atoms are omitted for clarity; phenyl and C_6F_5 groups are shown in wireframe for clarity; selected bond lengths [Å] and angles [°]: P1–C1 1.8036(18); P1–C7 1.8822(17); P1–C2 1.7475(16); P1–C6 1.7431(17); C2–C3 1.397(2); C3–C4 1.399(2); C5–C6 1.378(2); C7–N1 1.251(2); N1–B1 1.367(2); C7–C8 1.492(2); C1-P1-C7 102.58(8); P1-C7-N1 120.29(13); C7-N1-B1 172.06(18); C8-C7-N1 124.56(16).

deep green crystals in moderate yields (33–64%). The crystallographic characterisation of **3b** and **3c** revealed structures similar to that already discussed for **3a**, with essentially linear C–N–B arrangements and short B–N distances (for more details, see Supporting Information). Multinuclear NMR data of all compounds were also in line with those found for **3a**.

A slightly different outcome was observed using 2-(dimethylamino)acetonitrile (Scheme 3), which contains an additional pendant donor functionality, as was indicated by an immediate colour change from orange to deep pink (c.f. deep green for compounds **3a**–**3e**) upon addition of the substrate to a solution of **2** in diethyl ether. NMR analysis indicated the clean formation of a new product **4** that features a $^{31}P\{^{1}H\}$ resonance at δ(ppm) = −9.2, which is shifted to higher field relative to **3a**–**3e** (δ(ppm) = −1.0 to +0.6). The $^{11}B\{^{1}H\}$ signal (11.5 ppm for **4** versus 22–26 ppm for **3a**–**3e**) is also shifted to higher field, suggesting a different product structure, which was confirmed by single crystal X-ray diffraction (Figure 5). The molecular structure of **4** in the crystal reveals insertion of the nitrile into the P–B bond of **2** analogously to **3a**–**3e**. However, instead of a linear CNB moiety a five-membered Lewis adduct is formed in which the boron moiety interacts with both available nitrogen atoms. The rather elongated B1–N2 bond (1.7322(16) Å) of **4** is consistent with a dative interaction between B1 and the lone pair of N2. This interaction has a significant influence on the solid-state structure and spectroscopic properties of **4**. The crystallographic characterisation further shows that the C–N–B fragment is no longer linear (111.27(10)°) and the B1–N1 bond distance (1.5237(16) Å) is elongated compared to **3a** (1.367(2) Å). The UV–Vis spectrum of **4** shows an additional absorbance at λ = 523 nm, which explains the apparent colour change from green (for **3a**–**3e**) to pink.

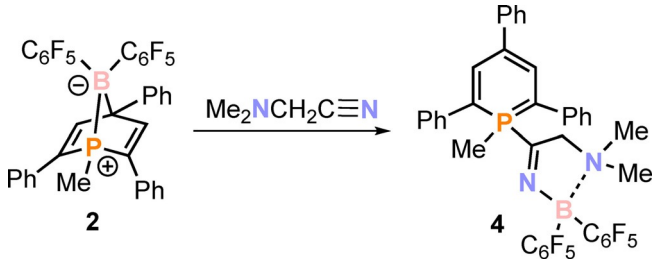

Scheme 3. Reaction of **2** with 2-(dimethylamino)acetonitrile.

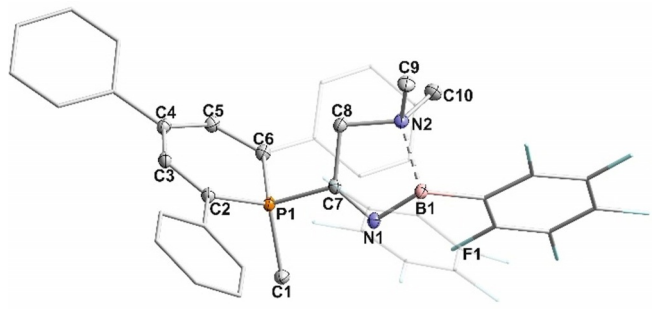

Figure 5. Molecular structure of **4** in the crystal. Displacement ellipsoids are shown at the 40% probability level; H atoms are omitted for clarity; phenyl and C_6F_5 groups are shown in wireframe for clarity; selected bond lengths [Å] and angles [°]: P1–C7 1.8435(12); P1–C2 1.7631(12); P1–C6 1.7612(12); P1–C1 1.8231(12); C2–C3 1.3916(17); C3–C4 1.3985(18); C4–C5 1.4070(17); C5–C6 1.3822(17); C7–C8 1.5084(16); N2–B1 1.7322(16); B1–N1 1.5237(16); N1–C7 1.2578(16); C7-N1-B1 111.27(10); N1-B1-N2 100.38(9); P1-C7-N1 125.34(9); C8-N2-B1 103.

To analyse the reaction course of **2** with nitriles in more detail, DFT calculations were again performed at the ωB97X-D/6–311 + G** level of theory (all energy values discussed are ΔG values in kcal mol^{-1}; see Figure 6 and vide supra). As already discussed, an initial ring opening of **2** forms isomer **Iso-2d**, which can act as an FLP for the activation of nitriles, modelled here using acetonitrile. This first step is consistent with the chemical exchange between **2** and **Iso-2d** suggested by ^{11}B NMR (Figure S84 and vide supra). Nitrile binding to the boron centre of **Iso-2d** then gives an adduct **Int-A** with almost identical energy. The subsequent rate-determining step involves cyclisation to give the high-energy bridged intermediate **Int-B** (this proceeds over an energy barrier of +21.5 kcal mol^{-1}, which is slightly higher than expected given the rapid reactivity observed at room temperature, but is nevertheless in satisfactory agreement with the experimental result, given the errors typically associated with the computational methods employed). This compound is highly unstable and rapidly rearranges with cleavage of the B–C bond. Flattening of the six-membered λ^5-phosphinine-derived ring gives initially **Int-C**, which readily isomerises through P–C bond rotation to the slightly more stable conformer **3a**, as is observed in the solid-state structure.

Reactivity of 2 toward alkynes

Encouraged by the high reactivity of **2** toward the strong, polar triple bond of nitriles, we were motivated to also test the reactivity of **2** toward the similarly strong, but apolar triple bonds of simple alkynes. The combination of **2** with one equivalent of phenylacetylene in benzene did not show any significant reactivity at room temperature. However, when heating this mixture to T = 60 °C overnight, the selective formation of a new product **5a** was observed (Scheme 4), indicated by the detection of a single new resonance in the $^{31}P\{^{1}H\}$ NMR spectrum at δ(ppm) = 1.7 (Figure S53 and Figure S54). This signal appears within the range observed for the nitrile activation products **3a**–**3e**, which suggests the formation of a similar tetracoordinate phosphorus environment. In contrast, the $^{11}B\{^{1}H\}$ NMR signal of **5a** is shifted to significantly higher field relative to **3a**–**3e** (−11.2 ppm for **5a** versus 22–26 ppm for **3a**–**3e**), and suggests a tetracoordinate rather than tricoordinate boron moiety (Figure S55).

The reactions of **2** with 4-(trifluoromethyl)- and 4-bromophenylacetylene led to analogous results, as the selective formation of the corresponding new compounds **5b** and **5c** was observed, which show very similar heteroatom NMR resonances ($^{31}P\{^{1}H\}$ δ(ppm) = 2.1 (**5b**), 1.9 (**5c**); $^{11}B\{^{1}H\}$ δ(ppm) = −11.2 (**5b**), −11.1 (**5c**)). Compounds **5a**–**5c** could be isolated as light red powders in good yields (up to 72%) by treatment of the crude product with *n*-hexane and thorough drying of the resulting

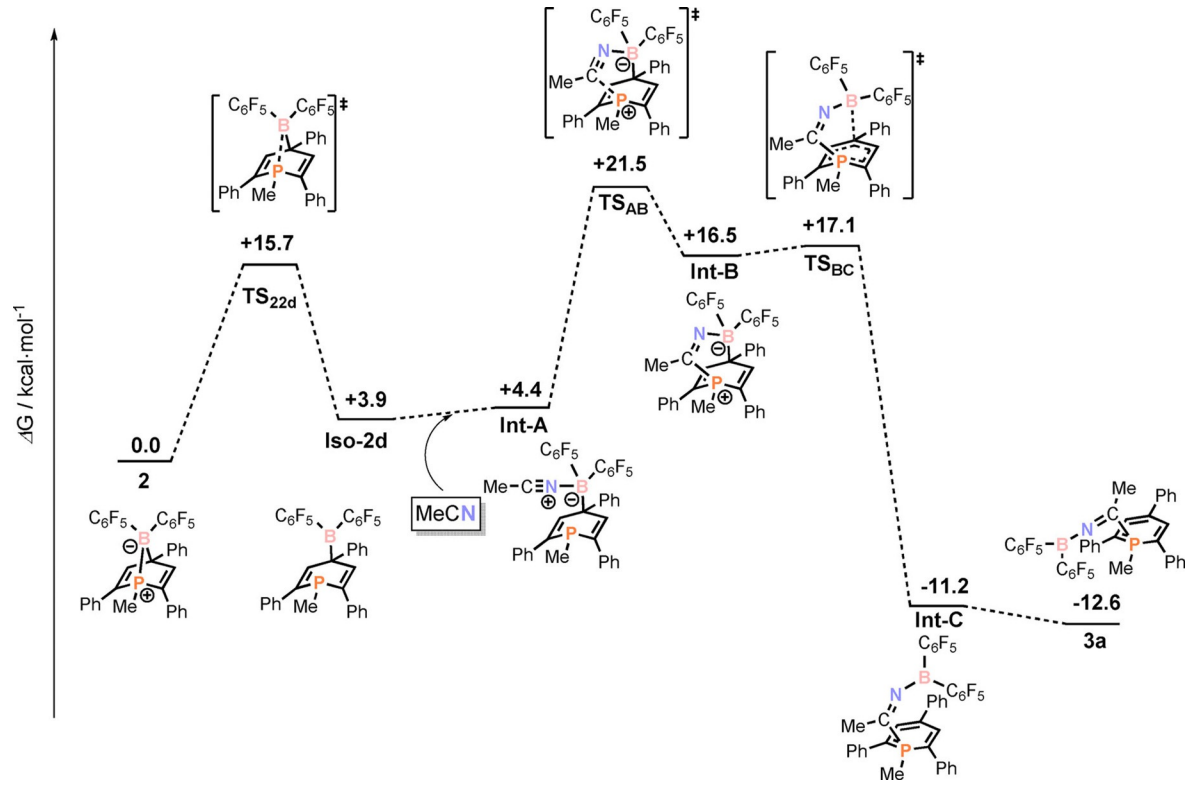

Figure 6. Relative ωB97X-D/6–311 + G** energies (calculated free energies ΔG in kcal mol^{-1}) for the conversion of **2** into **3 a**.

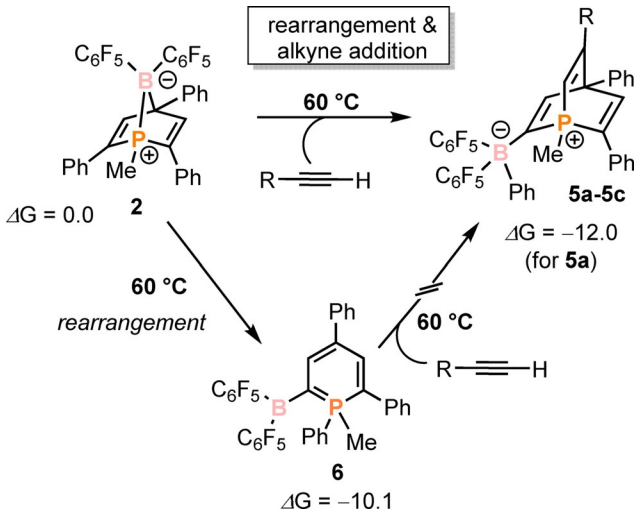

Scheme 4. Reaction of **2** with phenylacetylene derivatives, leading to the formation of **5 a**–**5 c**, thermal rearrangement of **2** to **6**, and relative ωB97X-D/6–311 + G** energies (calculated free energies ΔG in kcal mol^{-1}); **5 a**: R = Ph (61 %); **5 b**: R = 4-CF_3-C_6H_4 (62 %); **5 c**: R = 4-Br-C_6H_4 (72 %).

precipitate under vacuum. Single crystals of **5 b** and **5 c** were grown by slow evaporation of *n*-hexane solutions. The single crystal X-ray structures reveal the formation of a λ^4-1-phosphabarrelenium moiety, in which the alkyne bridges between P1 and C4 of the phosphinine-derived heterocycle.

As with nitriles, alkyne addition is accompanied by cleavage of both the P–B and C–B bonds of **2**. Remarkably, this is accompanied by migration of the $B(C_6F_5)_2$ moiety by formal insertion into the C2–Ph bond of **2**. Due to the modest quality of the structural data of **5 c** (Figure S106 and Table S2), only the structural data of **5 b** is discussed in detail here (Figure 7). The P1–C8 bond length (1.783(4) Å) is in the range of common P–C single bonds, whereas the C4–C7 bond (1.577(5) Å) is in the range of C–C single bonds.[18] The C2–C3, C5–C6 and C8–C7 distances are typical for C=C double bonds.[18]

The bond lengths and angles of **5 b** are consistent with other reported 1-phosphabarrelenes, except for P1–C8, which is slightly shortened (1.783(4) Å versus average 1.836 Å).[21] As a corollary, the angle C2-P1-C6 is also widened by roughly 8° compared to other 1-phosphabarrelenes (103.36(17)° vs. average 95.351°). These changes can be attributed to the tetracoordinate nature of the P atom, and were also observed for a selenium-substituted phosphabarrelene.[21a] Finally, the B1–C2 bond length in **5 b** (1.636(5) Å) is consistent with typical B–C single bonds.[14]

Typically, Diels–Alder type [4+2] cycloaddition of alkynes to neutral phosphinines to form 1-phosphabarrelenes must be performed using highly reactive arynes or activated alkynes (such as $F_3CC{\equiv}CCF_3$) as dienophiles.[21,22] That phospha-norbornadiene **2** reacts with simple phenylacetylenes under modest reaction conditions is therefore significant, and is reminiscent of the cationic 1-methyl-phosphininium salt [1-Me-2,6-$(SiMe_3)_2$-3,5-Ph_2-PC_5H][$GaCl_4$][23] that upon reaction with 4-octyne affords a 1-methyl-phosphabarrelenium tetrachlorogallate which was characterised by NMR spectroscopy.

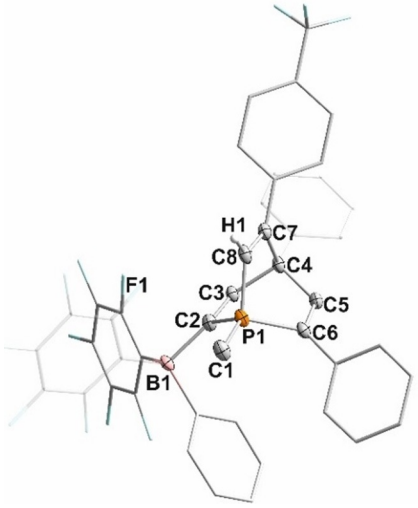

Figure 7. Molecular structure of **5b** in the crystal. Displacement ellipsoids are drawn at the 40% probability level; H atoms are omitted for clarity; phenyl; $C_6H_4CF_3$ and C_6F_5 groups are shown in wireframe for clarity; a disordered *n*-hexane molecule is omitted for clarity; selected bond lengths [Å] and angles [°]: P1–C8 1.783(4); C4–C7 1.577(5); P1–C2 1.799(4); P1–C6 1.816(4); P1–C1 1.781(4); C2–C3 1.335(5); C3–C4 1.560(5); C4–C5 1.541(5); C5–C6 1.335(5); C7–C8 1.334(5); C2–B1 1.636(5); P1-C8-C7 112.1(3); C8-C7-C4 116.4(3); C2-P1-C6 103.36(17); C3-C4-C5 107.2(3).

Although activation of alkynes is known to occur for other FLP systems, the concomitant $B(C_6F_5)_2$ migration observed in this case suggests an atypical activation mechanism.[20a–b, 24] To gain more insight, a solution of **2** was monitored by $^{31}P\{^1H\}$ NMR spectroscopy at 60 °C in the absence of alkyne, which resulted in the slow formation of a new species observed as a sharp singlet at δ(ppm) = +1.3 ppm (no analogous transformation was observed at RT). The chemical shift of this species is quite similar to those of **5a**–**5c** (δ(ppm) = 1.7–2.0), suggesting a similar environment at P. The structure of this species could not be determined by single crystal X-ray diffractometry; however, LIFDI–MS spectrometry, elemental analysis and NMR observations are consistent with the structure **6** depicted in Scheme 4. In particular, the calculated ^{31}P (δ(ppm) = +5 vs. +1.3 observed) and ^{11}B NMR (δ(ppm) = +43 vs. +54 observed) shifts of **6** are in agreement with the experimental data (Table S5). Additionally, the calculated and observed UV–Vis spectrum of **6** are in reasonable agreement (Figure S104 and S115).

VT $^{31}P\{^1H\}$ NMR monitoring of **2** was also carried out in the presence of an alkyne substrate. When 4-(trifluoromethyl)phenylacetylene was added to **2** at room temperature only a small singlet in the ^{31}P NMR spectrum at δ(ppm) = 1.4 ppm corresponding to the product **5b** could be observed next to the signals of **2** and **Iso-2a** (Figure S89). $^{31}P\{^1H\}$ NMR monitoring at 60 °C showed that **2** and **Iso-2a** convert quite selectively to the product **5b** (accompanied by generation of only 5% of **6**) within three hours (Figure S89), with no other observable intermediates. Notably, when the same alkyne was added to compound **6** at room temperature no reaction occurred, even upon heating to 60 °C. Thus, **6** does not appear to be an intermediate during the formation of **5a**–**5c**, but rather a competitive side-product that forms selectively in the absence of alkyne (Scheme 4, see Figure S114, Supporting Information, and the discussion in section S5.4 of the Supporting Information for further details).

Based on the structures of products **5** and **6**, it was anticipated that the observed reactivity might be proceeding through the isomeric form of **2**, **Iso-2c** (vide supra), in which the $B(C_6F_5)_2$ has migrated fully to the '*ortho*' position of the phosphorus heterocycle. This proposal is supported by DFT calculations which show that, following isomerisation to this 'open' form, a subsequent 1,2-phenyl migration can occur through $\mathbf{TS_{2CD}}$ (ΔG = 25 kcal mol^{-1}), which is accessible at elevated temperatures. This results in a zwitterionic methylphosphinium borate species **Int-D**. The alkyne subsequently adds to **Int-D** in a 1,4-manner forming **5a**,[23] in a step that can formally be considered as a hetero-Diels–Alder reaction. Alternatively, this step can be viewed as another FLP type reaction, in which the conjugated phosphorus heterocycle provides both the Lewis acidic and basic sites (c.f. **G**, Scheme 1) needed to activate the alkyne. In this interpretation it is expected that the aryl-substituted carbon atom from the phenylacetylene derivative should end up bound to the formally Lewis basic fragment of the FLP,[22b] due to better stabilisation of the positive charge that will accumulate on this carbon atom during the interaction of the alkyne with the Lewis acidic centre. Indeed, an alternative reaction pathway between **Int-D** and phenylacetylene to generate regioisomer **Int-E** was also calculated and it was found that although **Int-E** is thermodynamically slightly favoured over **5a**, the associated transition state $\mathbf{TS_{DE}}$ is significantly higher in energy than $\mathbf{TS_{D5a}}$ (+33.3 vs. +26.2 kcal mol^{-1}, see Figure 8). This implies that the phosphorus centre is the Lewis acidic site in this system, and "*para*-C4" is the Lewis basic site, which is consistent with the FLP type activation of dihydrogen by 1,3,5-triphosphinine derivatives.[9] Thus, the phenyl migration that transforms **Iso-2c** into **Int-D** results in an umpolung effect, in which the phosphorus centre changes in reactivity from nucleophilic (as observed in the activation of nitriles) to electrophilic (as observed in the activation of alkynes).

Conclusions

The unusual compound **2** incorporating a boron atom in a phospha-norbornadiene scaffold is readily accessible by reaction of a λ^4-phosphinine anion and a chloroborane. Even though **2** is nominally a classical Lewis acid–base adduct it shows FLP type reactivity due to its strained bicyclic structure, readily activating the C≡N triple bonds of various nitriles. These nitriles formally insert into the P–B bond, with concomitant splitting of the B–C bond, and ultimately connect to the resulting $B(C_6F_5)_2$ moiety in a linear fashion (**3a**–**3e**) unless an additional donor functionality is also present (as in **4**). DFT calculations revealed that these reactions proceed by a low energy ring-opening of the bridging norbornadiene P–B bond. Conversely, reactions of **2** with phenylacetylene derivatives afford phosphabarrelenes **5a**–**5c** by a mechanism that involves initial migration of $(C_6F_5)_2B$, through formal insertion into a

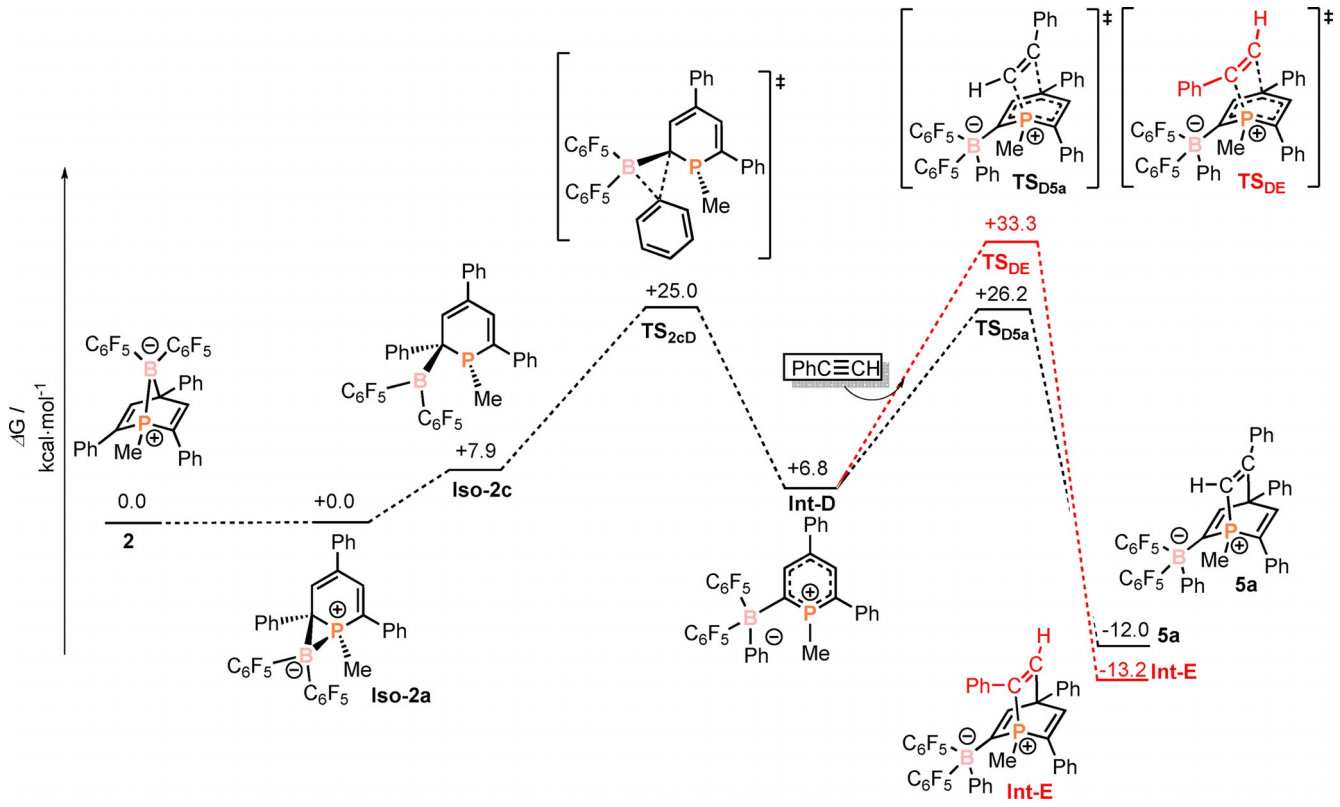

Figure 8. Relative ωB97X-D/6–311 + G** energies (calculated free energies ΔG in kcal mol^{-1}) for the conversion of **2** into **5a**.

C–C bond. This work highlights the ability of seemingly classical Lewis pairs to form reactive intermediates by reversible heterolytic element–element bond dissociation, while also illustrating the ability of phosphinine-derived Lewis bases to engage in interesting FLP reactivity that is not easily accessible using more conventional λ^3,σ^3-phosphines. The application of these principles to the activation of further small molecules is a worthwhile subject for future investigations.

Experimental Section

All experiments were performed under an atmosphere of dry argon by using standard glovebox techniques. Diethyl ether and *n*-hexane were purified, dried, and degassed with an MBraun SPS800 solvent purification system. NMR spectra were recorded on Bruker Avance 300 MHz and Avance 400 MHz spectrometers at 300 K and a Bruker Avance III HD 600 MHz spectrometer with a fluorine selective TBIF probe and a phosphorus selective TBIP probe at variable temperatures.^{1}H and ^{13}C{^{1}H} spectra were referenced internally to residual solvent resonances, while ^{31}P{^{1}H} and ^{31}P spectra were referenced externally to 85 % H_3PO_4(aq.). ^{11}B spectra were reference externally to $Et_2O{\cdot}BF_3$. ^{19}F spectra were referenced externally to $CFCl_3$. The assignment of ^{1}H and ^{13}C NMR signals was confirmed by two-dimensional (COSY, HSQC, and HMBC) experiments. For the chemical assignment 2,4,6-triphenylphosphinine will be referred to as TPP. UV–Vis spectra were recorded on a Varian Cary 50 spectrometer. Elemental analyses were determined by the analytical department of Regensburg University. Mass spectra were performed with Jeol AccuTOF GCX LIFDI-MS by the analytical department of Regensburg University. **1** was synthesised according to a literature procedure and $(C_6F_5)_2BCl$ was synthesised by an unpublished procedure.[2c] Nitriles and alkynes were purchased from Sigma–Aldrich and used as received.

X-ray Crystallography: The single-crystal X-ray diffraction data were recorded on an Agilent Technologies SuperNova and a GV1000, TitanS2 diffractometer with Cu-K_α radiation (λ = 1.54184 Å). Either semi-empirical multi-scan absorption corrections[25] or analytical ones[26] were applied to the data. The structures were solved with SHELXT[27] and least-square refinements on F^2 were carried out with SHELXL.[28] The hydrogen atoms were located in idealised positions and refined isotropically with a riding model.

CCDC 1946109 (for **2**), 1946111 (for **3a**), 1946112 (for **3b**), 1946114 (for **3c**), 1946115 (for **4**), 1946116 (for **5b**), and 1946118 contain the supplementary crystallographic data for this paper. These data are provided free of charge by The Cambridge Crystallographic Data Centre

Synthesis of 2

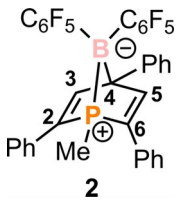

2

$(C_6F_5)_2BCl$ (171 mg, 0.45 mmol, 1 equiv) was dissolved in *n*-hexane (2 mL), cooled to −35 °C and slowly added to a suspension of **1** (200 mg, 0.45 mmol, 1 equiv) cooled to −35 °C in *n*-hexane (2 mL). An immediate colour change from deep pink to orange was observed. The orange suspension was stirred for 15 minutes and the precipitate was separated from the solution. The bright orange solid was extracted into diethyl ether (3×2 mL) and the solution was reduced in volume by half. After storage at −35 °C, **2** was isolated as a light orange powder. Yield 107 mg,

35%. Elemental analysis calcd for $C_{36}H_{20}BF_{10}P$ (Mw = 684.32 g mol^{-1}) C 63.19, H 2.95; found C 63.12, H 3.17. UV–Vis: (*n*-hexane, λ_{max}/nm, ε_{max}/L mol^{-1}·cm^{-1}): 221 (18278), 229 (15854), 290 (5399). ^{1}H NMR (400.13 MHz, 300 K, C_6D_6): δ = 1.47 (d, 3H, *Me*, $^2J_{PH}$ = 12.5 Hz), 6.91 (m, 4H, $C^{2,6}$-*H* of $C^{2,6}$-Ph), 7.04 (m, 6H, $C^{3,4,5}$-*H* of $C^{2,6}$-Ph), 7.20 (m, 3H, $C^{2,4,6}$-*H* of C^4-Ph), 7.27 (m, 2H, $C^{3,5}$-*H* of C^4-Ph), 7.56 ppm (d, 2H, $C^{3,5}$-*H* of TPP, $^3J_{PH}$ = 35 Hz). ^{13}C{^{1}H} NMR (100.61 MHz, 300 K, C_6D_6): δ = 1.5 (d, *Me*-TPP, $^1J_{CP}$ = 25 Hz), 64.3 (br, C^4 of TPP), 117.0 (br, C^1 of C_6F_5), 126.3 (s, C^4 of C^4-*Ph*), 127.2 (d, $C^{2,6}$ of $C^{2,6}$-*Ph*, $^3J_{CP}$ = 4 Hz), 127.4 (m, $C^{2,6}$ of C^4-*Ph*), 128.3 (s, $C^{3,5}$ of $C^{2,6}$-*Ph*), 129.3 (s, C^4 of $C^{2,6}$-*Ph*), 134.6 (d, C^1 of $C^{2,6}$-*Ph*, $^2J_{CP}$ = 5 Hz), 137.5 (br d, C_6F_5, $^1J_{FC}$ = 250 Hz), 137.9 (m, $C^{2,6}$ of TPP, $^1J_{CB}$ = 48 Hz), 140.1 (br d, C_6F_5, $^1J_{FC}$ = 260 Hz), 143.4 (d, C^1 of C^4-*Ph*, $J_{CF\ or\ CB}$ = 14 Hz), 147.5 (br d, C_6F_5, $^1J_{FC}$ = 244 Hz), 156.6 ppm (d, C^3 and C^5 of TPP, $^2J_{CP}$ = 17 Hz). ^{31}P{^{1}H} NMR (161.98 MHz, 300 K, C_6D_6): δ = 18.7 ppm (broad unresolved multiplet, the $^1J_{PB}$ could not be exactly determined to the line broadening ca.$^1J_{PB}$ = 60 Hz; minor **Iso-2a** is also observed). ^{31}P NMR (161.98 MHz, 300 K, C_6D_6): δ = 18.6 ppm (br m). ^{11}B{^{1}H} NMR (128.38 MHz, 300 K, C_6D_6): δ = 14.2 ppm (br s). ^{11}B NMR (128.38 MHz, 300 K, C_6D_6): δ = 14.1 ppm (bs). ^{19}F{^{1}H} NMR (376.66 MHz, 300 K, C_6D_6): δ = −156.4 (m, 4F), −163.0 (m, 6F). MS (LIFDI, toluene): *m/z* (%) = 684.10 M$^{+\cdot}$ (**2**); 339.12 ([1-Me-P($C_5H_2Ph_3$)]).

Synthesis of 3a–3e

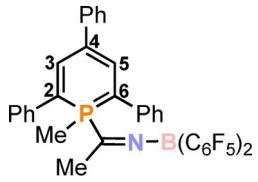

3a

Acetonitrile (4 µL, 0.059 mmol, 1 equiv) was added to a solution of **2** (40 mg, 0.059 mmol, 1 equiv) in diethyl ether (1 mL) at room temperature. An immediate colour change from orange to deep green was observed. The reaction mixture was stirred for 15 minutes, the solvent was completely removed, and the dark green oily residue was extracted with *n*-pentane (2×2 mL). After reducing the solution to half and storage at room temperature for 1 hour, **3a** could be isolated as dark green needles. Yield: 14 mg (33%). Elemental analysis calcd for $C_{38}H_{20}BF_{10}NP$ (Mw = 725.38 g mol^{-1}) C 62.92, H 3.20, N 1.93; found: C 63.28, H 3.31, N 1.42. UV–Vis: (*n*-hexane, λ_{max}/nm, ε_{max}/L mol^{-1}·cm^{-1}): 224 (41862), 253 (33000), 320sh (11060). ^{1}H NMR (400.13 MHz, 300 K, C_6D_6): δ = 1.74 (d, 3H, $^2J_{PH}$ = 13 Hz, *Me*-TPP), 2.09 (d, 3H, $^3J_{PH}$ = 8 Hz, *Me*CN), 6.94–7.13 (m, 11H, $H_{aromatic}$), 7.27 (m, 2H, $H_{aromatic}$), 7.41 (m, 2H, $H_{aromatic}$), 7.63 (s, 1H, $H_{aromatic}$), 7.70 ppm (s, 1H, $H_{aromatic}$). ^{13}C{^{1}H} NMR (100.61 MHz, 300 K, C_6D_6): δ = 9.0 (d, *Me*-TPP, $^1J_{CP}$ = 69 Hz), 24.4 (d, *Me*CN, $^2J_{CP}$ = 29 Hz), 82.0, 114.4, 124.5, 125.7, 127.0, 128.6, 128.7, 137.3, 139.4, 140.2, 142.8, 147.5, 156.9 ppm; due to the low signal to noise ratio, not all of the ^{13}C NMR signals were resolved.^{31}P{^{1}H} NMR (161.98 MHz, 300 K, C_6D_6): δ = 0.6 ppm (s). ^{31}P NMR (161.98 MHz, 300 K, C_6D_6): δ = 0.6 ppm (m). ^{11}B{^{1}H} NMR (128.38 MHz, 300 K, C_6D_6): δ = 21.9 ppm (br). ^{11}B NMR (128.38 MHz, 300 K, C_6D_6): δ = 21.4 ppm (br s). ^{19}F{^{1}H} NMR (376.66 MHz, 300 K, C_6D_6): δ = −131.8 (m, 4F), −151.07 (m, 2 F), −161.5 ppm (m, 4F).

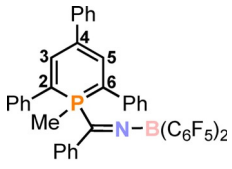

3b

Benzonitrile (7.5 µL, 0.073 mmol, 1 equiv) was added to a solution of **2** (50 mg, 0.073 mmol, 1 equiv) in diethyl ether (1 mL) at room temperature. An immediate colour change from orange to deep green was observed. The reaction mixture was stirred for 15 minutes, the solvent was completely removed, and the dark green oily residue was extracted with *n*-pentane (3×2 mL). After reducing the solution to half and storage at −35 °C for 1 hour, **3b** could be isolated as dark green needles. Yield: 37 mg (64%). Elemental analysis calcd for $C_{43}H_{25}BF_{10}NP$ (Mw = 787.45 g mol^{-1}) C 65.59, H 3.20, N 1.78; found: C 65.33, H 3.34, N 1.80. UV–Vis: (*n*-hexane, λ_{max}/nm, ε_{max}/L mol^{-1}·cm^{-1}): 259 (12766), 320sh (3979). ^{1}H NMR (400.13 MHz, 300 K, C_6D_6): δ = 2.00 (d, 3H, $^2J_{PH}$ = 13 Hz, *Me*-TPP), 6.89–7.11 (m, 15H, $H_{aromatic}$), 7.26 (m, 2H, $H_{aromatic}$), 7.38 (m, 2H, $H_{aromatic}$), 7.50 (s, 1H, $H_{aromatic}$), 7.59 (s, 1H, $H_{aromatic}$), 7.94 ppm (d, 1H, J = 8 Hz, $H_{aromatic}$). ^{13}C{^{1}H} NMR (100.61 MHz, 300 K, C_6D_6): δ = 12.10 (d, *Me*-TPP, $^1J_{CP}$ = 77 Hz), 85.6, 108.1, 115.1, 124.9, 125.1, 126.4, 128.8, 129.0, 129.4, 129.7, 132.0, 132.4, 132.7, 133.0, 137.7, 139.7, 140.2, 140.3, 148.0, 151.3 ppm; due to the low signal to noise ratio, not all of the ^{13}C NMR signals were resolved.. ^{31}P{^{1}H} NMR (161.98 MHz, 300 K, C_6D_6): δ = −0.1 (s). ^{31}P NMR (161.98 MHz, 300 K, C_6D_6): δ = −0.1 ppm (m). ^{11}B{^{1}H} NMR (128.38 MHz, 300 K, C_6D_6): δ = 23.0 ppm (bs). ^{11}B NMR (128.38 MHz, 300 K, C_6D_6): δ = 23.2 ppm (br s). ^{19}F{^{1}H} NMR (376.66 MHz, 300 K, C_6D_6): δ = −131.3 (m, 4F), −151.0 (m, 2 F), −161.2 ppm (m, 4F).

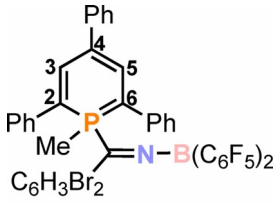

3c

3,5-Dibromobenzonitrile (19 mg, 0.073 mmol, 1 equiv) was added to a solution of **2** (50 mg, 0.073 mmol, 1 equiv) in diethyl ether (1 mL) at room temperature. An immediate colour change from orange to deep green was observed. The reaction mixture was stirred for 15 minutes, the solvent was completely removed, and the dark green oily residue was extracted with *n*-hexane (2 mL). After reducing the solution to half and storage at room temperature, **3c** could be isolated as dark green crystals. Yield: 30 mg (43%). Elemental analysis calcd for $C_{43}H_{23}BBr_2F_{10}NP$ (Mw = 945.24 g mol^{-1}) C 54.64, H 2.45, N 1.48; found: C 53.99, H 2.58, N 1.39. UV–Vis: (*n*-hexane, λ_{max}/nm, ε_{max}/L mol^{-1}·cm^{-1}): 260 (14990), 310sh (7040), 432 (2230). ^{1}H NMR (400.13 MHz, 300 K, C_6D_6): δ = 2.12 (d, 3H, $^2J_{PH}$ = 13 Hz, *Me*-TPP), 7.08–7.13 (m, 2H, $H_{aromatic}$), 7.15 (s, 4H, $H_{aromatic}$), 7.31–7.34 (m, 3H, $H_{aromatic}$), 7.45–7.50 (m, 3H, $H_{aromatic}$), 7.68 (m, 2H, $H_{aromatic}$), 7.73 (s, 1H, $H_{aromatic}$), 7.81 (s, 1H, $H_{aromatic}$), 8.19 ppm (s, 1H, $H_{aromatic}$). ^{13}C{^{1}H} NMR (100.61 MHz, 300 K, C_6D_6): δ = 11.5 (d, *Me*-TPP, $^1J_{CP}$ = 77 Hz), 84.9, 115.7, 124.2, 124.9, 125.3, 126.3, 128.6, 128.6, 130.9, 137.3, 137.9, 138.9, 140.1, 142.2, 147.5, 148.2 ppm; due to the low signal to noise ratio, not all of the ^{13}C NMR signals were resolved.. ^{31}P{^{1}H} NMR (161.98 MHz, 300 K, C_6D_6): δ = 0.6 ppm (s). ^{31}P NMR (161.98 MHz, 300 K, C_6D_6): δ = 0.6 ppm (m). ^{11}B{^{1}H} NMR (128.38 MHz, 300 K, C_6D_6): δ = 23.3 ppm (br s). ^{11}B NMR (128.38 MHz, 300 K, C_6D_6): δ = 23.6 ppm (br s). ^{19}F{^{1}H} NMR (376.66 MHz, 300 K, C_6D_6): δ = −131.3 (m, 4F), −150.2 (m, 2F), −160.8 ppm (m, 4F).

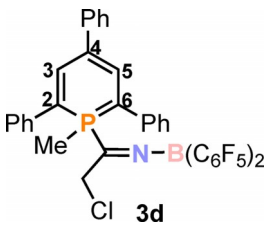

3d

2-Chloroacetonitrile (4.6 µL, 0.073 mmol, 1 equiv) was added to a solution of **2** (50 mg, 0.073 mmol, 1 equiv) in diethyl ether (1 mL) at room temperature. An immediate colour change from orange to deep green was observed. The reaction mixture was stirred for 15 minutes, the solvent was completely removed, and the dark green oily residue was extracted with *n*-hexane (3× 2 mL). After reducing the solution to half and storage at room tem-

perature, **3d** could be isolated as dark green solid. Yield: 22 mg (39%). Elemental analysis calcd for $C_{38}H_{22}BClF_{10}NP$ (Mw = 759.82 g mol^{-1}) C 60.07, H 2.92, N 1.84; found: C 60.46, H 3.27, N 1.23. UV–Vis: (*n*-hexane, λ_{max}/nm, ε_{max}/L mol^{-1}·cm^{-1}): 248 (22550), 307 (13470), 416 (6130). ^{1}H NMR (400.13 MHz, 300 K, C_6D_6): δ = 1.78 (d, 3H, $^2J_{PH}$ = 13 Hz, *Me*-TPP), 4.25 (s, CH_2CN), 6.97–7.13 (m, 11H, $H_{aromatic}$), 7.28 (m, 2H, $H_{aromatic}$), 7.36 (m, 2H, $H_{aromatic}$), 7.55 (s, 1H, $H_{aromatic}$), 7.63 ppm (s, 1H, $H_{aromatic}$). ^{13}C{^{1}H} NMR (100.61 MHz, 300 K, C_6D_6): δ = 10.1 (d, *Me*-TPP, $^1J_{CP}$ = 70 Hz), 45.8 (d, CH_2Cl, $^2J_{CP}$ = 42 Hz), 81.9, 115.0, 124.6, 124.8, 126.1, 126.9, 128.7, 137.2, 138.8, 139.9, 140.1, 147.8, 153.9 ppm; due to the low signal to noise ratio, not all of the ^{13}C NMR signals were resolved.. ^{31}P{^{1}H} NMR (161.98 MHz, 300 K, C_6D_6): δ = −1.0 ppm (s). ^{31}P NMR (161.98 MHz, 300 K, C_6D_6): δ = −1.0 ppm (m). ^{11}B{^{1}H} NMR (128.38 MHz, 300 K, C_6D_6): δ = 25.8 ppm (br s). ^{11}B NMR (128.38 MHz, 300 K, C_6D_6): δ = 25.8 ppm (br s). ^{19}F{^{1}H} NMR (376.66 MHz, 300 K, C_6D_6): δ = −131.1 (m, 4F), −150.2 (m, 2 F), −161.3 ppm (m, 4F).

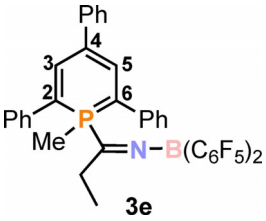

3e

Propionitrile (5.1 µL, 0.073 mmol, 1 equiv) was added to a solution of **2** (50 mg, 0.073 mmol, 1 equiv) in diethyl ether (1 mL) at room temperature. An immediate colour change from orange to deep green was observed. The reaction mixture was stirred for 15 minutes, the solvent was completely removed, and the dark green oily residue was extracted with *n*-hexane (2 mL). After reducing the solution to half and storage at room temperature, **3e** was isolated as dark green crystals. Yield: 22 mg (41%). Elemental analysis calcd for $C_{39}H_{25}BF_{10}NP$ (Mw = 739.40 g mol^{-1}) C 63.35, H 3.41, N 1.89; found: C 62.43, H 3.41, N 1.39. UV–Vis: (*n*-hexane, λ_{max}/nm, ε_{max}/L mol^{-1}·cm^{-1}): 259 (12766), 320sh (3979). ^{1}H NMR (400.13 MHz, 300 K, C_6D_6): δ = 0.93 (t, 3H, CH_2CH_3, $^3J_{HH}$ = 7 Hz), 1.89 (d, 3H, $^2J_{PH}$ = 13 Hz, *Me*-TPP), 2.65 (dq, 2H, CH_2CH_3, $^3J_{HH}$ = 7 Hz, $^3J_{PH}$ = 2.7 Hz), 7.06–7.23 (m, 11H, $H_{aromatic}$), 7.38 (m, 2H, $H_{aromatic}$), 7.53 (m, 2H, $H_{aromatic}$), 7.76 (s, 1H, $H_{aromatic}$), 7.84 ppm (s, 1H, $H_{aromatic}$). ^{13}C{^{1}H} NMR (100.61 MHz, 300 K, C_6D_6): δ = 8.0 (d, CH_2CH_3, $^3J_{CP}$ = 5 Hz), 8.8 (d, *Me*-TPP, $^1J_{CP}$ = 69 Hz), 29.6 (d, CH_2CH_3, $^2J_{CH}$ = 27 Hz), 82.2, 108.0, 114.2, 124.5, 124.5, 125.8, 127.0, 128.6, 128.7, 137.2, 139.4, 139.9, 142.0, 142.8, 147.6, 161.5 ppm; due to the low signal to noise ratio, not all of the ^{13}C NMR signals were resolved.. ^{31}P{^{1}H} NMR (161.98 MHz, 300 K, C_6D_6): δ = 0.1 (s). ^{31}P NMR (161.98 MHz, 300 K, C_6D_6): δ = 0.1 (m). ^{11}B{^{1}H} NMR (128.38 MHz, 300 K, C_6D_6): δ = 23.2 ppm (br s). ^{11}B NMR (128.38 MHz, 300 K, C_6D_6): δ = 23.2 ppm (br s). ^{19}F{^{1}H} NMR (376.66 MHz, 300 K, C_6D_6): δ = −131.7 (m, 4F), −151.2 (m, 2 F), −161.4 ppm (m, 4F).

Synthesis of 4

2-(Dimethylamino)acetonitrile (7.1 µL, 0.073 mmol, 1 equiv) was added to a solution of **2** (50 mg, 0.073 mmol, 1 equiv) in diethyl ether (1 mL) at room temperature. An immediate colour change from orange to deep pink was observed. The reaction mixture was stirred for 15 minutes, while a suspension with a pink solid was formed. The solution was decanted and the pink solid was washed with *n*-hexane (2×2 mL). **4** was isolated as a pink crystalline powder after drying under vacuum. Yield: 28 mg (50%). Elemental analysis calcd for $C_{40}H_{28}BF_{10}N_2P$ (Mw = 768.45 g mol^{-1}) C 62.52, H 3.67, N 3.65; found: C 62.41, H 3.60, N 3.49. UV–Vis: (diethyl ether, λ_{max}/nm, ε_{max}/L mol^{-1}·cm^{-1}): 260sh (17060), 316 (17420), 411 (4100), 523 (6644). ^{1}H NMR (400.13 MHz, 300 K, C_6D_6): δ = 1.39 (s, 6H, Me_2NCH_2CN), 2.05 (d, 3H, $^2J_{PH}$ = 13 Hz, *Me*-TPP), 3.43 (s, 2H, Me_2NCH_2CN), 6.97–7.00 (m, 2H, $H_{aromatic}$), 7.13 (m, 1H, $H_{aromatic}$), 7.17 (m, 4H, $H_{aromatic}$), 7.34–7.39 (m, 6H, $H_{aromatic}$), 7.67 (m, 2H, $H_{aromatic}$), 7.96 (s, 1H, $H_{aromatic}$), 8.03 ppm (s, 1H, $H_{aromatic}$). ^{13}C{^{1}H} NMR (100.61 MHz, 300 K, C_6D_6): δ = 12.7 (d, *Me*-TPP, $^1J_{CP}$ = 60 Hz), 48.8 (s, CH3 of NMe_2), 73.1 (br d, Me_2NCH_2CN, $^2J_{CP}$ = 40 Hz), 82.1, 113.8, 124.3, 124.4, 125.0, 125.6, 128.6, 128.8, 137.4, 137.5, 140.4, 143.5, 148.0, 165.7 ppm; due to the low signal to noise ratio, not all of the ^{13}C NMR signals were resolved.. ^{31}P{^{1}H} NMR (161.98 MHz, 300 K, C_6D_6): δ = −9.2 ppm (s). ^{31}P NMR (161.98 MHz, 300 K, C_6D_6): δ = −9.2 ppm (m). ^{11}B{^{1}H} NMR (128.38 MHz, 300 K, C_6D_6): δ = 11.5 ppm (br s). ^{11}B NMR (128.38 MHz, 300 K, C_6D_6): δ = 11.3 ppm (br s). ^{19}F{^{1}H} NMR (376.66 MHz, 300 K, C_6D_6): δ = −128.8 (m, 4F), −154.9 (m, 2 F), −162.5 ppm (m, 4F).

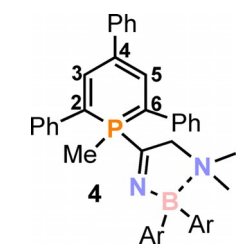

4

Synthesis of 5a–5c

Phenylacetylene (16 µL, 0.146 mmol, 1 equiv) was added to a solution of **2** (100 mg, 0.146 mmol, 1 equiv) in benzene (2 mL), the mixture was warmed up to 60 °C overnight. A colour change from orange to deep red was observed. After cooling down to room temperature, the solvent was completely removed. The remaining oily residue was triturated with *n*-hexane (2 mL). After drying under vacuum, **5a** was isolated as a light red powder. Yield: 70 mg (61%). Elemental analysis calcd for $C_{44}H_{26}BF_{10}P$ (Mw = 786.46 g mol^{-1}) C 67.20, H 3.33; found: C 66.52, H 3.51. UV–Vis: (diethyl ether, λ_{max}/nm, ε_{max}/L mol^{-1}·cm^{-1}): 451 (414). ^{1}H NMR (400.13 MHz, 300 K, C_6D_6): δ = 1.20 (d, 3H, $^2J_{PH}$ = 15 Hz, *Me*-TPP), 6.05 (d, 1H, $^2J_{PH}$ = 22 Hz, PC*H*=C−), 6.36 (m, 2H, $H_{aromatic}$), 6.58 (m, 2H, $H_{aromatic}$), 6.76–6.87 (m, 5H, $H_{aromatic}$), 7.02–7.18 (m, 7H, $H_{aromatic}$), 7.36 (m, 2H, $H_{aromatic}$), 7.58 (s, 1H, $H_{aromatic}$), 7.65 ppm (s, 1H, $H_{aromatic}$). ^{13}C{^{1}H} NMR (100.61 MHz, 300 K, C_6D_6): δ = −0.3 (d, *Me*-TPP, $^1J_{CP}$ = 52 Hz), 66.4 (d, HC*C*Ph, $^2J_{CP}$ = 45 Hz), 120.8 (d, HCCPh, $^1J_{CP}$ = 67 Hz), 125.1, 127.2, 128.1, 128.5, 128.7, 128.8, 129.00, 132.1, 135.0, 136.9, 139.5, 148.3, 150.4 ppm; due to the low signal to noise ratio, not all of the ^{13}C NMR signals were resolved.. ^{31}P{^{1}H} NMR (161.98 MHz, 300 K, C_6D_6): δ = 1.7 ppm (s). ^{31}P NMR (161.98 MHz, 300 K, C_6D_6): δ = 1.7 ppm (s). ^{11}B{^{1}H} NMR (128.38 MHz, 300 K, C_6D_6): δ = −11.2 ppm (s). ^{11}B NMR (128.38 MHz, 300 K, C_6D_6): δ = −11.2 ppm (s). ^{19}F{^{1}H} NMR (376.66 MHz, 300 K, C_6D_6): δ = −128.2 (m, 4F), −159.4 (m, 2 F), −164.0 ppm (m, 4F).

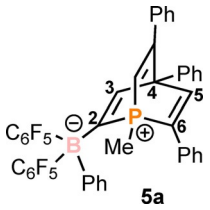

5a

4-(Trifluoromethyl)phenylacetylene (24 µL, 0.146 mmol, 1 equiv) was added to a solution of **2** (100 mg, 0.146 mmol, 1 equiv) in benzene (2 mL), the mixture was warmed up to 60 °C overnight. A colour change from orange to deep red was observed. After cooling down to room temperature, the solvent was completely removed. The remaining oily residue was triturated with *n*-hexane (2 mL). After drying under vacuum, **5b** was isolated as a light red powder. Yield: 77 mg (62%). Elemental analysis calcd for $C_{45}H_{25}BF_{13}P$ (Mw = 854.46 g mol^{-1}) C 63.26, H 2.95; found: C 63.58, H 3.30. UV–Vis: (di-

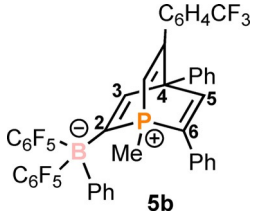

5b

ethyl ether, λ_{max}/nm, ε_{max}/L mol^{-1}·cm^{-1}): 467 (431). ^{1}H NMR (400.13 MHz, 300 K, C_6D_6): δ = 1.19 (s, 3H, *Me*-TPP), 6.00 (d, 1H, $^{2}J_{PH}$ = 23 Hz, PC*H*=C–), 6.35 (m, 2H, $H_{aromatic}$), 6.46 (m, 2H, $H_{aromatic}$), 6.74–6.82 (m, 3H, $H_{aromatic}$), 6.98–7.17 (m, 9H, $H_{aromatic}$), 7.33 (m, 2H, $H_{aromatic}$), 7.50 (s, 1H, $H_{aromatic}$), 7.58 ppm (s, 1H, $H_{aromatic}$). ^{13}C{^{1}H} NMR (100.61 MHz, 300 K, C_6D_6): δ = −0.33 (d, *Me*-TPP, $^{1}J_{CP}$ = 52 Hz), 66.0, 122.4, 124.5, 125.2, 125.4, 128.5, 128.7, 128.8, 129.2, 129.9, 130.3, 131.8, 135.0, 138.8, 140.3, 141.3, 148.3, 150.0, 171.8 ppm; due to the low signal to noise ratio, not all of the ^{13}C NMR signals were resolved.. ^{31}P{^{1}H} NMR (161.98 MHz, 300 K, C_6D_6): δ = 2.1 ppm (s). ^{31}P NMR (161.98 MHz, 300 K, C_6D_6): δ = 2.1 ppm (s). ^{11}B{^{1}H} NMR (128.38 MHz, 300 K, C_6D_6): δ = −11.2 ppm (s). ^{11}B NMR (128.38 MHz, 300 K, C_6D_6): δ = −11.2 ppm (s). ^{19}F{^{1}H} NMR (376.66 MHz, 300 K, C_6D_6): δ = −62.7 (s, 3F, CF_3), −128.4 (m, 2F, C_6F_5), −159.1 (m, 2 F, C_6F_5), −163.9 ppm (m, 4F, C_6F_5).

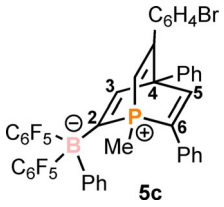

5c

4-Bromophenylacetylene (26 mg, 0.146 mmol, 1 equiv) was added to a solution of **2** (100 mg, 0.146 mmol, 1 equiv) in benzene (2 mL), the mixture was warmed up to 60 °C overnight. A colour change from orange to deep red was observed. After cooling down to room temperature, the solvent was completely removed. The remaining oily residue was triturated with *n*-hexane (2 mL). After drying under vacuum, **5c** was isolated as a light red powder. Yield: 91 mg (72%). Elemental analysis calcd for $C_{44}H_{25}BBrF_{10}P$ (Mw = 865.36 g mol^{-1}) C 61.07, H 2.91; found: C 64.45, H 3.42. UV–Vis: (diethyl ether, λ_{max}/nm, ε_{max}/L mol^{-1}·cm^{-1}): 470 (500). ^{1}H NMR (400.13 MHz, 300 K, C_6D_6): δ = 1.19 (s, 3H, *Me*-TPP), 5.98 (d, 1H, $^{2}J_{PH}$ = 23 Hz, PC*H*=C–), 6.27 (m, 2H, $H_{aromatic}$), 6.34 (m, 2H, $H_{aromatic}$), 6.77–6.82 (m, 3H, $H_{aromatic}$), 6.95 (m, 3H, $H_{aromatic}$), 7.00–7.08 (m, 6H, $H_{aromatic}$), 7.33 (m, 2H, $H_{aromatic}$), 7.51 (s, 1H, $H_{aromatic}$), 7.58 ppm (s, 1H, $H_{aromatic}$). ^{13}C{^{1}H} NMR (100.61 MHz, 300 K, C_6D_6): δ = −0.3 (d, *Me*-TPP, $^{1}J_{CP}$ = 53 Hz), 66.0, 121.3, 122.8, 125.2, 128.6, 128.7, 128.8, 129.1, 130.9, 131.5, 131.9, 133.4, 135.0, 135.6, 135.7, 139.1, 148.4, 150.0, 172.2 ppm; due to the low signal to noise ratio, not all of the ^{13}C NMR signals were resolved.. ^{31}P{^{1}H} NMR (161.98 MHz, 300 K, C_6D_6): δ = 1.9 ppm (s). ^{31}P NMR (161.98 MHz, 300 K, C_6D_6): δ = 1.9 ppm (s). ^{11}B{^{1}H} NMR (128.38 MHz, 300 K, C_6D_6): δ = −11.2 ppm (s). ^{11}B NMR (128.38 MHz, 300 K, C_6D_6): δ = −11.2 ppm (s). ^{19}F{^{1}H} NMR (376.66 MHz, 300 K, C_6D_6): δ = −128.1 (m, 2F), −159.3 (m, 2 F), −164.0 ppm (m, 4F).

Synthesis of 6

2 (50 mg, 0.073 mmol) was dissolved in benzene (0.5 mL) and heated to 60 °C over two days. The solvent of the deep red reaction mixture was completely evaporated, and the remaining red oily residue was extracted with *n*-hexane (2 x2 mL). After slow evaporation at room temperature and recrystallisation from *n*-hexane, **6** could be isolated as a deep red crystalline solid. Yield 18 mg, 36%. Elemental analysis calcd for $C_{36}H_{20}BF_{10}P$ (Mw = 684.32 g mol^{-1}) C 63.19, H 2.95; found C 63.54, H 3.17. UV–Vis: (diethyl ether, λ_{max}/nm, ε_{max}/L mol^{-1}·cm^{-1}): 270 (22251), 490 (9017).

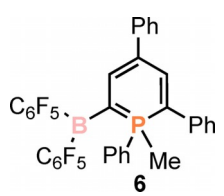

6

^{1}H NMR (400.13 MHz, 300 K, C_6D_6): δ = 1.65 (d, 3H, $^{2}J_{PH}$ = 14 Hz), 6.96 (m, 9H, $H_{aromatic}$), 7.11 (m, 2H, $H_{aromatic}$), 7.33 (m, 2H, $H_{aromatic}$), 7.54 (m, 3H, $H_{aromatic}$), 8.04 ppm (m, 1H, $H_{aromatic}$). ^{13}C{^{1}H} NMR (100.61 MHz, 300 K, C_6D_6): δ = 125.4, 125.7, 126.8, 126.9, 128.7, 128.9, 128.9, 137.7, 137.7, 142.2, 146.4, 146.5, 146.6 ppm; due to the low signal to noise ratio, not all of the ^{13}C NMR signals were resolved.. ^{31}P{^{1}H} NMR (161.98 MHz, 300 K, C_6D_6): δ = 1.7 ppm (s). ^{31}P NMR (161.98 MHz, 300 K, C_6D_6): δ = 1.8 ppm. ^{11}B{^{1}H} NMR (128.38 MHz, 300 K, C_6D_6): δ = 54.2 ppm (br s). ^{11}B NMR (128.38 MHz, 300 K, C_6D_6): δ = 54.4 ppm (br s). ^{19}F{^{1}H} NMR (376.66 MHz, 300 K, C_6D_6): δ = −129.3 (m), −130.3 (s), −133 (m), −144.7 (m), −154.8 (m), −159.5 (s), −160.8 (s), −161.9 (s), −162.7 ppm (s). MS (LIFDI, toluene): *m/z* (%) = 684.14 м$^{+\cdot}$ (**6**).

Acknowledgements

Funding by the Deutsche Forschungsgemeinschaft (WO1496/9-1 and MU1657/5-1) is gratefully acknowledged. J.C.S. and D.J.S. acknowledge the Alexander von Humboldt Foundation for Humboldt Research Fellowships. A.R.J. is grateful for the support of a Veni grant from the Netherlands Organisation for Scientific Research (NWO).

Conflict of interest

The authors declare no conflict of interest.

Keywords: alkyne · frustrated Lewis pair · nitrile · norbornadiene · phosphinine

[1] a) G. Märkl, *Angew. Chem.* **1966**, *78*, 907–908; b) A. Moores, L. Ricard, P. Le Floch, N. Mézailles, *Organometallics* **2003**, *22*, 1960–1966; c) A. J. Ashe, *Acc. Chem. Res.* **1978**, *11*, 153–157; d) A. J. Ashe, T. W. Smith, *Tetrahedron Lett.* **1977**, *18*, 407–410.

[2] a) G. Märkl, A. Merz, *Tetrahedron Lett.* **1968**, *9*, 3611–3614; b) G. Märkl, A. Merz, *Tetrahedron Lett.* **1971**, *12*, 1215–1218; c) G. Märkl, F. Lieb, A. Merz, *Angew. Chem. Int. Ed. Engl.* **1967**, *6*, 87–88; *Angew. Chem.* **1967**, *79*, 59–59.

[3] a) G. Märkl, C. Martin, W. Weber, *Tetrahedron Lett.* **1981**, *22*, 1207–1210; b) M. Bruce, G. Meissner, M. Weber, J. Wiecko, C. Müller, *Eur. J. Inorg. Chem.* **2014**, 1719–1726.

[4] a) A. Moores, N. Mézailles, L. Ricard, Y. Jean, P. Le Floch, *Organometallics* **2004**, *23*, 2870–2875; b) A. Moores, N. Mézailles, L. Ricard, P. Le Floch, *Organometallics* **2005**, *24*, 508–513; c) M. Dochnahl, M. Doux, E. Faillard, L. Ricard, P. L. Floch, *Eur. J. Inorg. Chem.* **2005**, 125–134; d) M. Bruce, *Doctoral Thesis*, Freie Universität Berlin, Berlin, **2016**; e) M. Doux, N. Mézailles, M. Melaimi, L. Ricard, P. Le Floch, *Chem. Commun.* **2002**, 1566–1567.

[5] a) B. Rezaei Rad, U. Chakraborty, B. Mühldorf, J. A. W. Sklorz, M. Bodensteiner, C. Müller, R. Wolf, *Organometallics* **2015**, *34*, 622–635; b) C. M. Hoidn, R. Wolf, *Dalton Trans.* **2016**, *45*, 8875–8884; c) C. M. Hoidn, J. Leitl, C. G. P. Ziegler, I. G. Shenderovich, R. Wolf, *Eur. J. Inorg. Chem.* **2019**, 1567–1574.

[6] D. W. Stephan, *J. Am. Chem. Soc.* **2015**, *137*, 10018–10032.

[7] G. C. Welch, R. R. San Juan, J. D. Masuda, D. W. Stephan, *Science* **2006**, *314*, 1124–1126.

[8] a) R. Liu, X. Liu, K. Ouyang, Q. Yan, *ACS Macro Lett.* **2019**, *8*, 200–204; b) C. M. Mömming, E. Otten, G. Kehr, R. Fröhlich, S. Grimme, D. W. Stephan, G. Erker, *Angew. Chem. Int. Ed.* **2009**, *48*, 6643–6646; *Angew. Chem.* **2009**, *121*, 6770–6773.

[9] L. E. Longobardi, C. A. Russell, M. Green, N. S. Townsend, K. Wang, A. J. Holmes, S. B. Duckett, J. E. McGrady, D. W. Stephan, *J. Am. Chem. Soc.* **2014**, *136*, 13453–13457.

[10] a) D. Neibecker, R. Réau, *Angew. Chem. Int. Ed. Engl.* **1989**, *28*, 500–501; *Angew. Chem.* **1989**, *101*, 479–480; b) M. Siutkowski, F. Mercier, L. Ricard, F. Mathey, *Organometallics* **2006**, *25*, 2585–2589.

[11] a) J. H. Barnard, S. Yruegas, S. A. Couchman, D. J. D. Wilson, J. L. Dutton, C. D. Martin, *Organometallics* **2016**, *35*, 929–931; b) S. Dong, L. Wang, T.

Wang, C. G. Daniliuc, M. Brinkkötter, H. Eckert, G. Kehr, G. Erker, *Dalton Trans.* **2018**, *47*, 4449 – 4454.
[12] a) U. Rohde, F. Ruthe, P. G. Jones, R. Streubel, *Angew. Chem. Int. Ed.* **1999**, *38*, 215 – 217; *Angew. Chem.* **1999**, *111*, 158 – 160; b) A. Koner, B. M. Gabidullin, Z. Kelemen, L. Nyulászi, G. I. Nikonov, R. Streubel, *Dalton Trans.* **2019**, *48*, 8248 – 8253.
[13] F. Mathey, *Chem. Rev.* **1988**, *88*, 429 – 453.
[14] P. Pyykkö, M. Atsumi, *Chem. Eur. J.* **2009**, *15*, 186 – 197.
[15] a) F. Ge, G. Kehr, C. G. Daniliuc, G. Erker, *Organometallics* **2015**, *34*, 229 – 235; b) C. Fan, W. E. Piers, M. Parvez, R. McDonald, *Organometallics* **2010**, *29*, 5132 – 5139; c) F. Ge, G. Kehr, C. G. Daniliuc, G. Erker, *J. Am. Chem. Soc.* **2014**, *136*, 68 – 71.
[16] a) C. P. Sindlinger, F. S. W. Aicher, H. Schubert, L. Wesemann, *Angew. Chem. Int. Ed.* **2017**, *56*, 2198 – 2202; *Angew. Chem.* **2017**, *129*, 2232 – 2236; b) J. Schneider, C. P. Sindlinger, S. M. Freitag, H. Schubert, L. Wesemann, *Angew. Chem.* **2017**, *129*, 339 – 343.
[17] H. Braunschweig, J. Maier, K. Radacki, J. Wahler, *Organometallics* **2013**, *32*, 6353 – 6359.
[18] P. Pyykkö, M. Atsumi, *Chem. Eur. J.* **2009**, *15*, 12770 – 12779.
[19] a) L. J. Hounjet, C. Bannwarth, C. N. Garon, C. B. Caputo, S. Grimme, D. W. Stephan, *Angew. Chem. Int. Ed.* **2013**, *52*, 7492 – 7495; *Angew. Chem.* **2013**, *125*, 7640 – 7643; b) R. Dobrovetsky, K. Takeuchi, D. W. Stephan, *Chem. Commun.* **2015**, *51*, 2396 – 2398; c) L. Wu, S. S. Chitnis, H. Jiao, V. T. Annibale, I. Manners, *J. Am. Chem. Soc.* **2017**, *139*, 16780 – 16790; d) R. Dobrovetsky, D. W. Stephan, *J. Am. Chem. Soc.* **2013**, *135*, 4974 – 4977; e) D. J. Scott, M. J. Fuchter, A. E. Ashley, *Angew. Chem. Int. Ed.* **2014**, *53*, 10218 – 10222; *Angew. Chem.* **2014**, *126*, 10382 – 10386.
[20] a) K. Samigullin, I. Georg, M. Bolte, H.-W. Lerner, M. Wagner, *Chem. Eur. J.* **2016**, *22*, 3478 – 3484; b) E. R. M. Habraken, L. C. Mens, M. Nieger, M. Lutz, A. W. Ehlers, J. C. Slootweg, *Dalton Trans.* **2017**, *46*, 12284 – 12292; c) J. Möricke, B. Wibbeling, C. G. Daniliuc, G. Kehr, G. Erker, *Philos. Trans. R. Soc. Math. Phys. Eng. Sci.* **2017**, *375*, 20170015.
[21] a) M. Rigo, J. A. W. Sklorz, N. Hatje, F. Noack, M. Weber, J. Wiecko, C. Müller, *Dalton Trans.* **2016**, *45*, 2218 – 2226; b) B. Breit, E. Fuchs, *Chem. Commun.* **2004**, *0*, 694 – 695; c) M. Blug, C. Guibert, X.-F. Le Goff, N. Mézailles, P. Le Floch, *Chem. Commun.* **2008**, 201 – 203.
[22] a) G. Märkl, F. Lieb, C. Martin, *Tetrahedron Lett.* **1971**, *12*, 1249 – 1252; b) E. Fuchs, M. Keller, B. Breit, *Chem. Eur. J.* **2006**, *12*, 6930 – 6939; c) M. Rigo, E. R. M. Habraken, K. Bhattacharyya, M. Weber, A. W. Ehlers, N. Mézailles, J. C. Slootweg, C. Müller, *Chem. Eur. J.* **2019**, *25*, 8769 – 8779.
[23] A. Moores, L. Ricard, P. L. Floch, *Angew. Chem. Int. Ed.* **2003**, *42*, 4940 – 4944; *Angew. Chem.* **2003**, *115*, 5090 – 5094.
[24] a) K. Chernichenko, Á. Madarász, I. Pápai, M. Nieger, M. Leskelä, T. Repo, *Nat. Chem.* **2013**, *5*, 718 – 723; b) C. Jiang, O. Blacque, H. Berke, *Organometallics* **2010**, *29*, 125 – 133; c) M. A. Dureen, C. C. Brown, D. W. Stephan, *Organometallics* **2010**, *29*, 6594 – 6607; d) R. L. Melen, L. C. Wilkins, B. M. Kariuki, H. Wadepohl, L. H. Gade, A. S. K. Hashmi, D. W. Stephan, M. M. Hansmann, *Organometallics* **2015**, *34*, 4127 – 4137; e) V. Fasano, L. D. Curless, J. E. Radcliffe, M. J. Ingleson, *Angew. Chem. Int. Ed.* **2017**, *56*, 9202 – 9206; *Angew. Chem.* **2017**, *129*, 9330 – 9334; f) C. Chen, R. Fröhlich, G. Kehr, G. Erker, *Chem. Commun.* **2010**, *46*, 3580 – 3582; g) J. Li, C. G. Daniliuc, G. Kehr, G. Erker, *Chem. Commun.* **2018**, *54*, 6344 – 6347; h) M. A. Dureen, D. W. Stephan, *J. Am. Chem. Soc.* **2009**, *131*, 8396 – 8397; i) T. Wang, X. Jentgens, C. G. Daniliuc, G. Kehr, G. Erker, *ChemCatChem* **2017**, *9*, 651 – 658.
[25] a) SCALE3ABS, CrysAlisPro, Aglient Technologies Inc., Oxford, GB, **2012**; b) G. M. Sheldrick, SADABS, Bruker AXS, Madison, USA, **2007**.
[26] R. C. Clark, J. S. Reid, *Acta Crystallogr. Sect. A* **1995**, *51*, 887 – 897.
[27] G. M. Sheldrick, *Acta Crystallogr. Sect. C* **2015**, *71*, 3 – 8.
[28] G. M. Sheldrick, *Acta Crystallogr. Sect. A* **2008**, *64*, 112 – 122.

Manuscript received: January 16, 2020
Revised manuscript received: February 12, 2020
Accepted manuscript online: February 13, 2020
Version of record online: May 29, 2020

